

Article

Combined Magnesia, Ceria and Nickel catalyst supported over γ -Alumina Doped with Titania for Dry Reforming of Methane

Ahmed Sadeq Al-Fatesh ^{1,*}, Samsudeen Olajide Kasim ¹, Ahmed Aidid Ibrahim ¹,
Anis Hamza Fakeeha ¹, Ahmed Elhag Abasaheed ¹, Rasheed Alrasheed ², Rawan Ashamari ² and
Abdulaziz Bagabas ^{2,*}

¹ Chemical Engineering Department, College of Engineering, King Saud University, P.O. Box 800, Riyadh 11421, Saudi Arabia; sofkolajide2@gmail.com (S.O.K.); aidid@ksu.edu.sa (A.A.I.); anishf@ksu.edu.sa (A.H.F.); abasaheed@ksu.edu.sa (A.E.A.)

² National Petrochemical Technology Center (NPTC), Materials Science Research Institute (MSRI), King Abdulaziz City for Science and Technology, P.O. Box 6086, Riyadh 11442, Saudi Arabia; rrisheed@kacst.edu.sa (R.A.); ralshammary@kacst.edu.sa (R.A.)

* Correspondence: aalfatesh@ksu.edu.sa (A.S.A.-F.), abagabas@hotmail.com (A.B.); Tel.: +966-11-467-6859 (A.S.A.-F.); Tel.: +966-11-481-3790 (A.B.)

Received: 21 January 2019; Accepted: 13 February 2019; Published: 18 February 2019



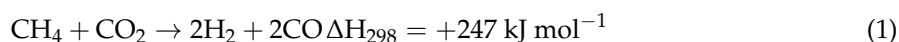
Abstract: This study investigated dry reforming of methane (DRM) over combined catalysts supported on γ -Al₂O₃ support doped with 3.0 wt. % TiO₂. Physicochemical properties of all catalysts were determined by inductively coupled plasma/mass spectrometry (ICP-MS), nitrogen physisorption, X-ray diffraction, temperature programmed reduction/oxidation/desorption/pulse hydrogen chemisorption, thermogravimetric analysis, and scanning electron microscopy. Addition of CeO₂ and MgO to Ni strengthened the interaction between the Ni and the support. The catalytic activity results indicate that the addition of CeO₂ and MgO to Ni did not reduce carbon deposition, but improved the activity of the catalysts. Temperature programmed oxidation (TPO) revealed the formation of carbon that is mainly amorphous and small amount of graphite. The highest CH₄ and CO₂ conversion was found for the catalyst composed of 5.0 wt. % NiO-10.0 wt. % CeO₂/3.0 wt. %TiO₂- γ -Al₂O₃ (Ti-CAT-II), resulting in H₂/CO mole ratio close to unity. The optimum reaction conditions in terms of reactant conversion and H₂/CO mole ratio were achieved by varying space velocity and CO₂/CH₄ mole ratio.

Keywords: CH₄; CeO₂; dry reforming; MgO; Ni; TiO₂

1. Introduction

Global warming has become an alarming issue. Emissions of greenhouse gases including carbon dioxide (CO₂) and methane (CH₄) actively contribute to global warming. Methods of transforming these CO₂(g) and CH₄(g) into useful products are an important area of study to generate industrially important fuels and chemicals [1–3]. In this context, numerous reforming reactions of CH₄ have been employed using several oxidants (e.g., H₂O, CO₂, O₂, etc.) to produce H₂(g) or synthesis gas (syngas, a mixture of H₂(g) and CO(g)) with an equimolar ratio of H₂(g)/CO(g). Methane reforming processes include steam reforming, auto thermal reforming, tri-reforming, etc. [4–11]. Methane reforming using CO₂, known as dry reforming (DRM), is attractive because it mitigates the emission of CH₄ and CO₂, produces syngas, the starting material in the Fischer-Tropsch process to generate hydrocarbons and oxygenates, and generates clean energy through the combustion of hydrogen [12]. CH₄ is a

cost-effective feedstock for syngas production. The primary reaction that governs the process is as follows:



The reaction is energetically unfavorable, thus requiring high temperatures to achieve acceptable conversion. Both noble metals (i.e., Ru, Rh, or Pt) and first-row transition metals (i.e., Ni, Fe, Co) are common active elements in that catalyze CO_2 reforming of CH_4 . Although noble metals display high activity and stability, their limited availability and high price have rendered them inappropriate for industrial use [13,14]. On the other hand, the first-row transition metals are cheaper and possess similar activity, but their stability is hampered by carbon deposition and particle sintering [15–18]. Therefore, development of Ni-based catalysts with high activity and resistance to deactivation due to carbon formation and metal sintering is essential for DRM. Catalytic performance can be influenced by many factors such as the active metal, support type, and texture. The support can enhance the catalyst selectivity, activity, and stability by increasing the surface area and dispersion of the active metal [19]. For example, Ni deposited on alumina supports result in high catalytic activity, but rapidly deactivates due to sintering, coke deposition, and formation of surface nickel aluminate phase. To increase the catalytic performance of Ni/ γ - Al_2O_3 , various parameters can be incorporated in the catalyst.

Titania (TiO_2) is characterized by low specific surface area and poor mechanical strength, and undergoes a phase transformation from anatase to rutile at high temperatures, making it unsuitable for high temperature reactions [20]. Previous studies have shown enhanced thermal stabilization of TiO_2 by introducing a thermally stable second metal oxide (i.e., SiO_2 , Al_2O_3 , etc.) [21,22]. Incorporation of TiO_2 in Al_2O_3 supports can improve metal dispersion, reduce particle sintering, increase thermal stability, and enhance oxygen storage capacity to assist in gasifying carbon produced in reforming reaction [23]. Tauster et al. investigated the effects of support modification on the oxidation state of Ru and the catalytic performance of Ru/ TiO_2 catalysts under conditions of partial oxidation of methane. It was found that doping of TiO_2 with small amounts of WO_3 favored oxygen adsorption on Ru under reaction conditions, resulting in a stabilization of a fraction of the catalyst in its oxidized form [24]. Addition of metal oxide promoters has been used to improve Ni metal catalysts. For instance, Shamskar et al. investigated the addition of CeO_2 , La_2O_3 , and ZrO_2 to Ni/ Al_2O_3 catalyst used for DRM and found that ceria-promoted catalyst reduced the carbon formation [25]. Ni-MgO- Al_2O_3 catalysts were used for steam reforming of methane by Jang et al. [26]. Al-Fatesh et al. studied the promotional effect of ceria in the catalytic DRM and found that the Ni doping with ceria resulted in an excellent activity and lowered coke formation [27]. MgO promoters enhance CH_4 conversion and mitigated the effect of the potassium poisoning of the Ni-based catalyst. The MgO promoter is beneficial in suppressing carbon formation.

In the present work, supported combinations of MgO, CeO_2 and NiO catalysts were developed to retain high activity and stability while reducing the formation of coke during DRM. The effect of using MgO and CeO_2 as separate and combined promoters, for 5.0 wt. % NiO supported over γ - Al_2O_3 doped with 3.0 wt. % TiO_2 was studied. We determine the impact of each modifier on observed catalytic performance.

2. Results and Discussion

2.1. X-ray Powder Diffraction (XRD)

The XRD patterns of all the fresh catalysts are displayed in Figure S1 in the electronic supplementary information (ESI). All the patterns consisted of various metal oxides, where the presence metal oxide phases depended on the added components used to prepare the catalysts. Three metal oxides existed in all catalysts, where these metal oxides were the component of the support: cubic gamma-aluminum oxide, γ - $(\text{Al}_2\text{O}_3)_{1.333}$ (PDF 01-075-0921), cubic synthesized honguiite titanium oxide, $(\text{TiO}_{0.8})_{0.913}$ (PDF 01-085-1380), and aluminum silicate, $\text{Al}_{0.5}\text{Si}_{0.75}\text{O}_{2.25}$ (PDF 00-037-1460). Rhombohedral nickel oxide, NiO (PDF 00-044-1159) was found in Ti-CAT-I, Ti-CAT-II, Ti-CAT-III, and

Ti-CAT-V (these notations are defined in Section 3.2). When magnesium was added, cubic magnesium nickel oxide, MgNiO_2 (PDF 00-024-0712) formed. Cubic synthesized cerianite (Ce) (ceria), CeO_2 (PDF 00-034-0394), was detected in Ti-CAT-I, Ti-CAT-II, Ti-CAT-IV, and Ti-CAT-VI. Addition of magnesium strongly influenced the interaction of cerium with the other components of the catalyst. Monoclinic magnesium cerium oxide, MgCeO_3 (PDF 00-004-0641), and cubic magnesium cerium titanium oxide, $\text{Mg}_2\text{CeTiO}_6$ (PDF 00-058-0550) were present in Ti-CAT-I and Ti-CAT-IV. Cubic periclase magnesium oxide, MgO (PDF 01-071-1176) was detected in Ti-CAT-I, Ti-CAT-III, and Ti-CAT-IV.

2.2. Inductively Coupled Plasma Mass Spectroscopy (ICP-MS)

ICP-MS analysis was carried out to quantify the metallic components as metal oxides for the best two catalysts. The results are shown in Table 1a,b.

Table 1 summarizes the results of ICP analysis of the metallic components in the prepared catalysts and compares it with the theoretical values. The experimental results were found to be in excellent agreement with the nominal values.

Table 1. ICP metal oxide microanalysis of Ti-CAT.

(a)						
Catalyst Component	Ti-CAT-I					
	NiO	CeO₂	MgO	TiO₂	SiO₂	Al₂O₃
Theoretical, wt/wt. %	5.00	10.00	1.00	3.00	2.00	79.00
Experimental, wt/wt. %	5.21	9.91	1.02	2.86	1.93	78.05
(b)						
Catalyst Component	Ti-CAT-II					
	NiO	CeO₂	MgO	TiO₂	SiO₂	Al₂O₃
Theoretical, wt/wt. %	5.00	10.00	0.00	3.00	2.00	79.00
Experimental, wt/wt. %	4.98	10.11	0.00	2.92	2.07	81.03

2.3. Temperature Programmed Desorption (CO₂-TPD)

The CO₂-TPD experiment was performed to study the basicity of the catalysts. The results obtained are shown in Figure 1. The basicity of the catalyst has a paramount influence on the catalytic performance in DRM due to the acidic nature of CO₂. Thus, strong basic sites can enhance catalytic activity and increase the chemisorption and reaction of reacting gases [28]. Distribution of basic sites on the catalyst (i.e., weak, intermediate, strong, and very strong) correspond to the different desorption peaks in the temperature ranges of 20–150, 150–300, 300–450, and >450 °C, respectively, in the CO₂-TPD profile [29,30].

All catalysts, except Ti-CAT-V and Ti-CAT-VI, showed the same basic site classification, because the CO₂ desorption peaks appeared at almost the same different temperature ranges (Figure 1). Both Ti-CAT-V and Ti-CAT-VI have basic sites corresponding to site of high and strong basicity centered at a temperature around 310 °C.

For the peaks appearing at different temperature ranges, peaks in the temperature range of 50–125 °C correspond to weak basic sites, peaks at 160–185 °C fall under the category of intermediate strength basic sites, while the peaks at 260 °C correspond to strong basicity sites. An elbow peak was observed for all of the samples, except for Ti-CAT-V and Ti-CAT-VI, at temperature centered around 500 °C. This peak had no significant CO₂ uptake.

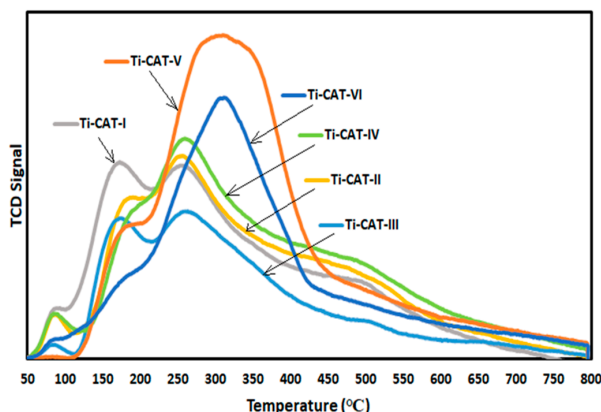


Figure 1. CO₂-TPD profiles of the synthesized catalysts.

2.4. Surface Characterization

The textural properties of the fresh catalysts were studied using nitrogen adsorption-desorption isotherms. The results obtained from the N₂ physisorption are shown in Table 2 and that of the isotherms are presented in Figure 2. The results give an insight into the variations in the activities of the catalysts. In accordance to IUPAC classifications of isotherms, the isotherms in Figure 2 fall under the category of type II, with an H3-type hysteresis loop, which results from capillary condensation and evaporation at high relative pressures [31].

Table 2. N₂ physisorption results for the different catalysts.

Catalyst	BET Surface Area (m ² /g)	Av. Pore Diameter (nm)	Pore Volume (cm ³ /g)
Ti-CAT-I	284	11.5	0.40
Ti-CAT-II	283	12.4	0.43
Ti-CAT-III	326	11.8	0.43
Ti-CAT-IV	256	12.3	0.39
Ti-CAT-V	334	12.4	0.43
Ti-CAT-VI	299	12.5	0.40

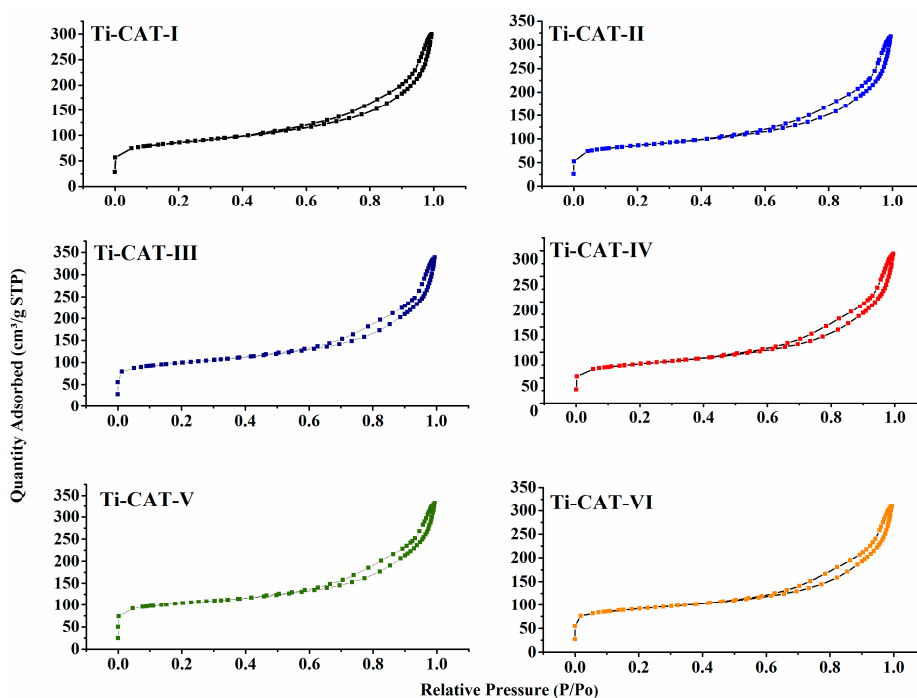


Figure 2. Cont.

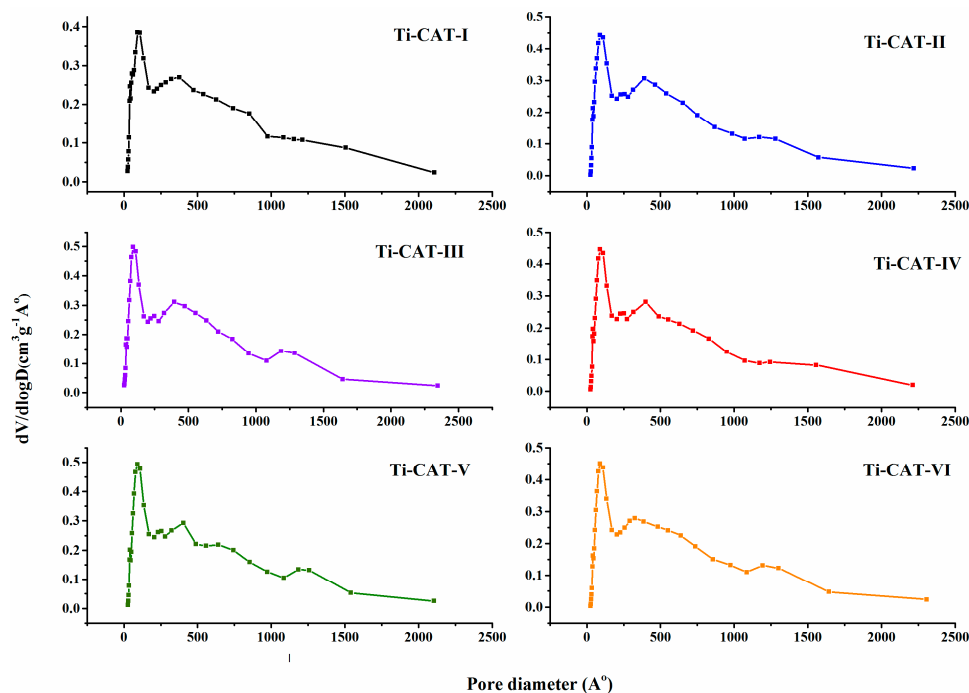


Figure 2. N₂ adsorption-desorption isotherms and BJH desorption pore size distribution curves for Ti-CAT samples.

Type II isotherms constitute macroporous adsorbents, and for detailed study, the BJH pore size distribution is represented in Figure 2. All the Ti-CAT samples displayed a bimodal mesoporous/macroporous distribution curve with average pore size in the range 11.5–12.5 nm, typical for macroporous adsorbents with large surface area. For example, Jiang et al. [32] and Zhao et al. [33] synthesized macro-mesoporous bimodal titania with high surface areas. Here, the effect of surface area variation is observed when Mg, Ce, and Ni were combined. Table 2 shows that surface areas of the combined metal catalysts are reduced in relation to single-metal component catalysts. This observation is due to the combined metal deposition on the porous structure of the support and filling pores [34].

2.5. H₂-TPR

The reduction behavior of the different catalyst samples was investigated using H₂-TPR and the profiles are presented in Figure 3. The nickel reduction peaks for Ti-CAT-*x* (*x* = I, II, III) samples containing Ni combined with other metals, are characterized by three reduction regions at low, medium and high temperature ranges. Their ranges are dependent on the degree of dispersion and interaction of the active metal with the support. The nickel phase reducibility was influenced by the combination of the metal oxides. The reduction peak in the temperature range of 280–380 °C is assigned to the reduction of NiO having weak interaction with the support. Higher temperature peaks (600–700 °C) are likely due to the reduction of NiO species having strong interactions with the support. The reduction peak of Ni²⁺ derived from spinel is found at around 810 °C [35].

For Ti-CAT-V (the catalyst with only Ni), the NiO reduction peaks appeared narrower and more intense in temperature ranges lower than those of combined metal counterparts.

Only two reduction peaks are observed for Ti-CAT-VI at temperature ranges centered at 260 and 325 °C. Similar reduction peaks are expected for CeO₂ promoted samples, but appear to have merged with the peaks for NiO that appeared around that temperature range.

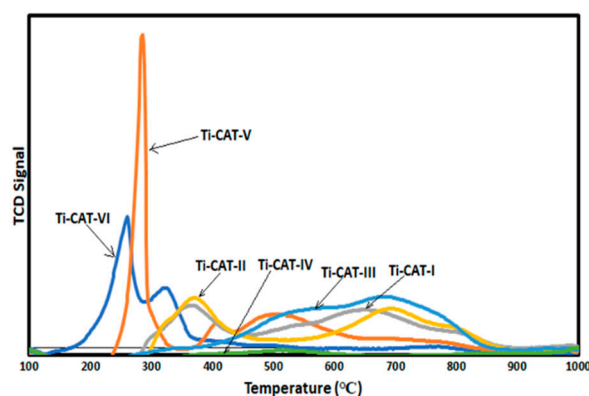


Figure 3. TPR profiles of the promoted and un-promoted catalysts.

2.6. Effect of MgO and CeO₂ Combination on the Catalytic Performance

The effects of combining CeO₂ and MgO on Ti-CAT-V and their catalytic performance were studied by comparing the activities of Ti-CAT-V catalyst with that of Ti-CAT-I, Ti-CAT-II, and Ti-CAT-III. CH₄, CO₂ conversions, H₂/CO mole ratio, and their selectivity at 700 °C, for 7.0 h time-on-stream for DRM were calculated and plotted as shown in Figure 4. All the promoted catalysts have CH₄ and CO₂ conversions higher than that of the Ti-CAT-V catalyst except for Ti-CAT-VI and Ti-CAT-IV, which showed no sign of reaction during the DRM. Ti-CAT-II had the highest CH₄ conversion at the start of the reaction (~55%) and maintained stability at around 52%. The high specific surface area of the catalyst (283 m²/g) enhanced the adsorption, diffusion, and contact of the reactant gases. The high average pore diameter and pore volume of Ti-CAT-II is a likely factor for the best-in-class performance. The Ce and Mg promoted catalysts enhanced the activity. The improvement of the activity is accompanied by the formation of graphitic carbon in comparison with the unpromoted catalysts, as depicted in the TG analysis.

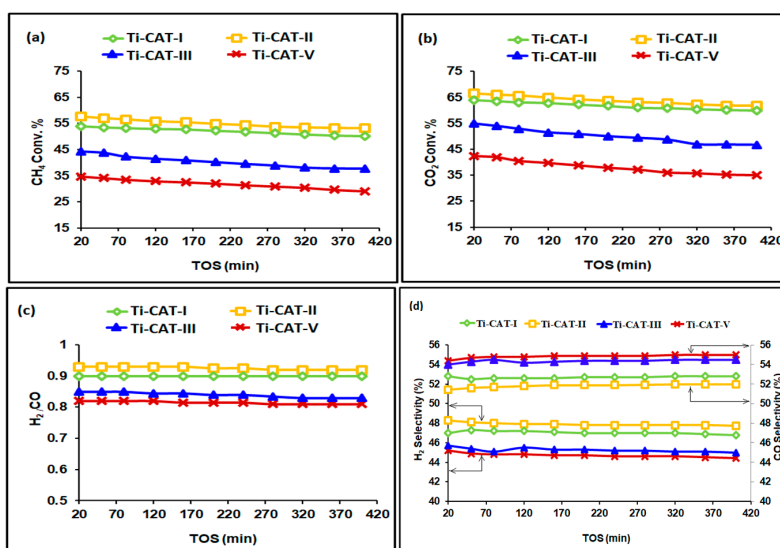


Figure 4. Catalytic performance of Ti-CAT-I, Ti-CAT-II, Ti-CAT-III, and Ti-CAT-V (a) CH₄ conversion (b) CO₂ conversion and (c) H₂/CO ratio and (d) H₂, CO selectivity.

The same trend was observed for CO₂ conversion, with the Ti-Cat-V catalyst showing the least conversion. For all the catalysts under investigation, CO₂ conversion was observed to be higher than CH₄ conversion, which is suggestive of the occurrence of reverse water gas shift (RWGS) reaction. Wang et al. gave the same observation in their study on catalytic hydrogenation of carbon dioxide [36].



In addition, the H₂/CO mole ratio showed values less than 1 for all the catalysts. The deviation from the stoichiometric ratio is also suggestive of the occurrence of RWGS reaction. Ti-CAT-II appeared to be the most selective towards H₂ (~48%) and least selective towards CO (~52%), while Ti-CAT-V has the least H₂ selectivity (~45%) but the highest CO selectivity (~55%). In all cases, the as-prepared catalysts showed higher CO selectivity than H₂.

Ti-CAT-II catalyst resulted in a H₂/CO mole ratio value closest to 1, compared to the tested catalysts. The desirable value of the syngas ratio suitable for downstream Fischer-Tropsch synthesis is unity [37], thus making it the best option for the dry reforming.

2.7. H₂-Pulse Chemisorption

To understand the effect of the active Ni component on the catalytic performance of the best two catalysts, Ti-CAT-I and Ti-CAT-II, we carried out H₂ pulse chemisorption to determine the degree of Ni dispersion on the surface of the support and Ni metallic surface area. The results of H₂-pulse chemisorption are displayed in Table 3. We found that both catalysts had high Ni metallic surface areas of ~90% and good dispersion of ~13%, which is responsible for the good catalytic performance of the two catalysts. The small relative higher catalytic performance of Ti-CAT-II than that of Ti-CAT-I could be attributed to the slightly higher Ni metallic surface area and dispersion of Ti-CAT-II.

Table 3. Ni metallic surface area and dispersion obtained by H₂ chemisorption.

Catalyst	Ni Metallic Surface Area, m ² /g	Ni Dispersion, %
Ti-CAT-I	89	13.3
Ti-CAT-II	91	13.6

2.8. Temperature Programmed Oxidation (TPO) of the Spent Catalysts

TPO is a useful technique that can be employed to determine the nature of the carbon deposited onto the surface of the catalysts. Several forms of carbon deposition have been reported in dry reforming reactions—ranging from atomic carbon, to graphitic, and amorphous carbon. The carbon can undergo gasification to form CO₂ under oxidative atmosphere and at different temperature ranges. The atomic carbon, amorphous, and graphitic carbon can be gasified at temperatures less than 250, 250–600, and >600 °C, respectively [38]. The TPO profiles of Ti-CAT-I and Ti-CAT-II spent catalysts are shown in Figure 5. Each of the catalysts exhibited a broad peak near 600 °C and a low-intensity shoulder at 100–250 °C. According to the TPO results, the carbon deposited on both Ti-CAT-I and Ti-CAT-II spent catalysts revealed the formation of carbon atoms, mostly amorphous carbon, and a small amount of extent graphitic carbon.

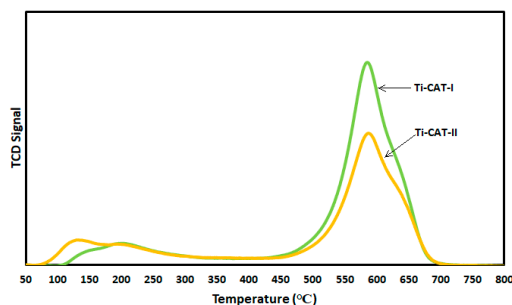


Figure 5. TPO profiles for both Ti-CAT-I and Ti-CAT-II.

2.9. SEM and TG Analysis

We used scanning electron microscopy (SEM) to determine the change in morphology of the spent catalysts. Figure 6 shows the SEM micrographs for the best two catalysts: Ti-CAT-I and Ti-CAT-II. Similar morphology, based on agglomerated, spherical nanoparticles, was observed for both fresh catalysts (Figure 6A,B). Such an observation was expected, because both catalysts were synthesized using an identical preparation procedure and had similar components.

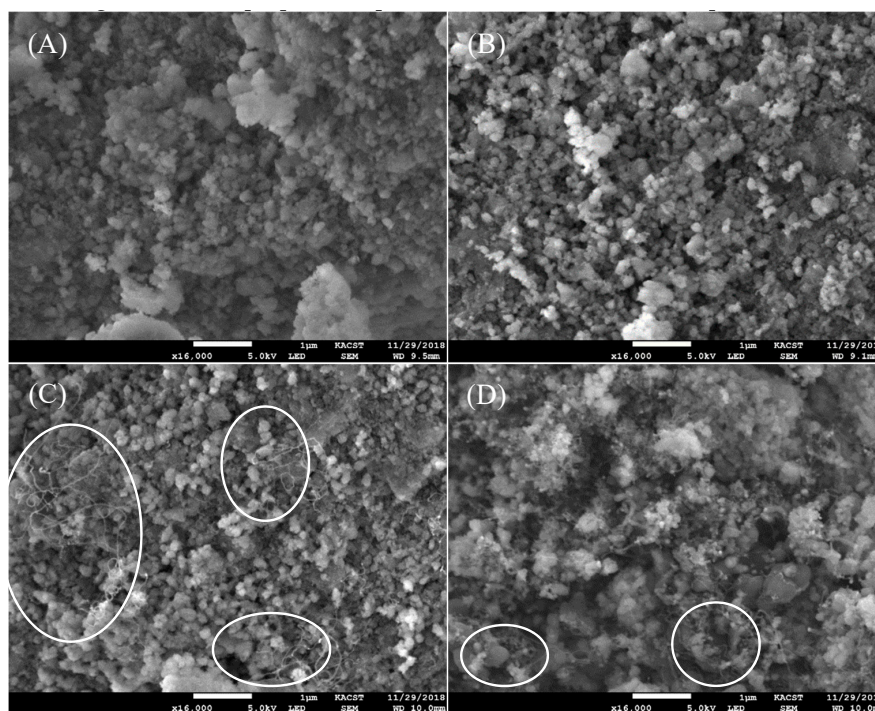


Figure 6. SEM micrographs for fresh catalysts (A) Ti-CAT-I, (B) Ti-CAT-II, and spent catalysts (C) Ti-CAT-I, (D) Ti-CAT-II. White circles are for some areas where CNTs are present.

The morphology of the spent catalysts was similar to that one of the fresh samples, except for the presence of carbon nanotubes (CNTs) on the surface of the spent catalysts (Figure 6C,D). Detection of CNTs on the surface of the spent catalyst is in agreement with the TPO results (c.f. Figure 5) and confirms the results of TGA of spent catalysts (Figure 7). The presence of CNTs on the surface of the spent catalysts could be attributed to Boudouard reaction, which in turn would be responsible for reducing the catalytic performance.

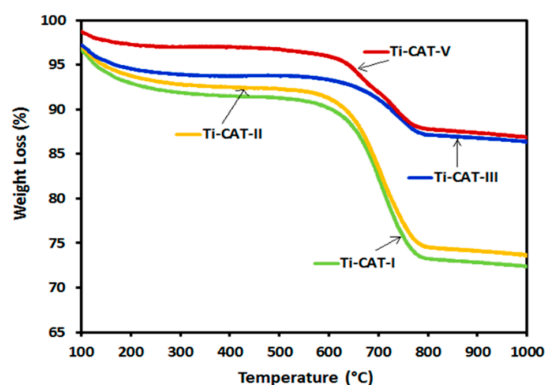


Figure 7. TGA profiles for the spent catalysts.

After the 7 h reaction, we analyzed the used catalysts by thermal gravimetric analysis (TGA), a quantitative analysis that determines the amount of carbon deposition. Figure 7 shows the result of the analysis. Catalysts that showed no sign of reaction were not reported. The weight loss (%) for virtually all the catalysts began at around 620 °C. The TGA profiles revealed that both Ti-CAT-V and Ti-CAT-III catalysts had the lowest weight loss, ~15.0%, while the two most reactive catalysts (Ti-CAT-II and Ti-CAT-I) had the highest amount of carbon deposition, corresponding to a weight loss of 25.0%.

From these TGA results of spent catalysts, it can be inferred that the combined metal catalysts, namely Ti-CAT-II and Ti-CAT-I, enhance the feed conversion capacity of the catalysts and gasify the carbon deposited over the surface to a considerable extent.

2.10. Effect of Space Velocity

The effect of gas hourly space velocity (GHSV) was studied on the catalyst that showed the best performance in the previous section (i.e., Ti-CAT-II catalyst). GHSV of 19,500 and 78,000 $\frac{\text{feed flow rate}}{\text{mass of cat.}} \left(\frac{\text{mL}}{\text{g} \cdot \text{h}} \right)$ were considered at 700 °C and time-on-stream over 7.0 h for DRM, while keeping the mass of the catalyst constant. These GHSV values are half and twice as much as the initial GHSV of 39,000 $\text{mL g}^{-1} \text{h}^{-1}$, respectively. The results, in terms of CO₂ and CH₄ conversions, as well as H₂/CO mole ratio, were calculated and plotted in Figure 8A,B. As the GHSV increased, the CH₄ and CO₂ conversions decreased, with the highest conversions for both CH₄ and CO₂ being obtained at a GHSV of 19,500 $\frac{\text{feed flow rate}}{\text{mass of cat.}} \left(\frac{\text{mL}}{\text{g} \cdot \text{h}} \right)$. The decrease in conversions can be attributed to the feed having less residence time at higher GHSV [39]. A similar trend was observed with H₂/CO mole ratio, where it decreased from a ratio of 1 to ~0.8. However, the results at GHSV of 39,000 were the most stable in comparison to those obtained at other GHSV values.

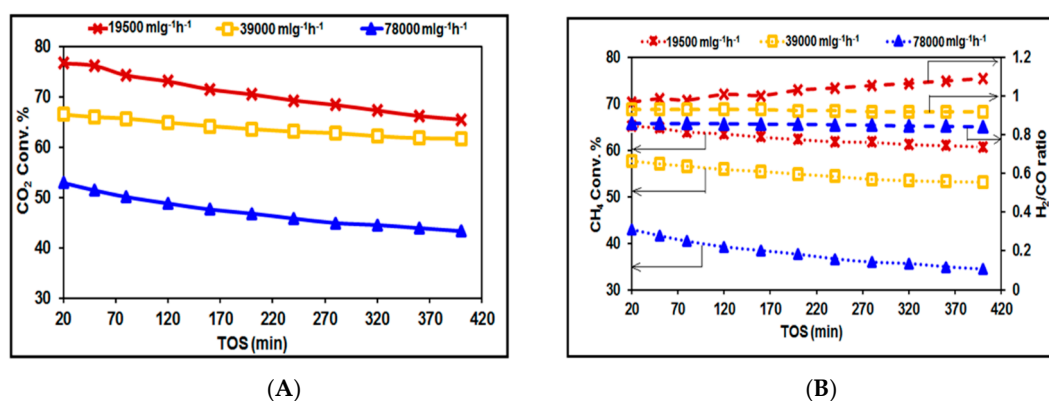


Figure 8. (A) CO₂ conversion for Ti-CAT-II at different gas hourly space velocity (B) CH₄ and H₂/CO ratio for Ti-CAT-II catalyst at different space velocities.

2.11. Effect of GHSV on Carbon Deposition

Quantitative analysis of carbon deposition was performed on the catalyst Ti-CAT-II used in methane dry reforming at 3 different space velocities 19,500, 39,000 and 78,000 $\text{mL g}^{-1} \text{h}^{-1}$.

The results obtained after the completion of the reactions are shown in Figure 9. The analysis for the reaction performed at 19,500 $\text{mL g}^{-1} \text{h}^{-1}$ showed the least amount of carbon deposition of about 18%, which shows that, relatively, more contact time between the catalyst and the feed stream was allowed at this space velocity, giving room for gasification of the coke that was deposited during the reaction. The reactions carried out at 39,000 and 78,000 $\text{mL g}^{-1} \text{h}^{-1}$ showed higher carbon deposition of about 26 and 25%, respectively. This is an indication that at the higher space velocities, the residence time was not enough for the gasification of the carbon deposit, which variably continued to pile up. Lalit et al. reported similar findings in their study of the effect of GHSV on the conversion of CH₄ and CO₂ [39].

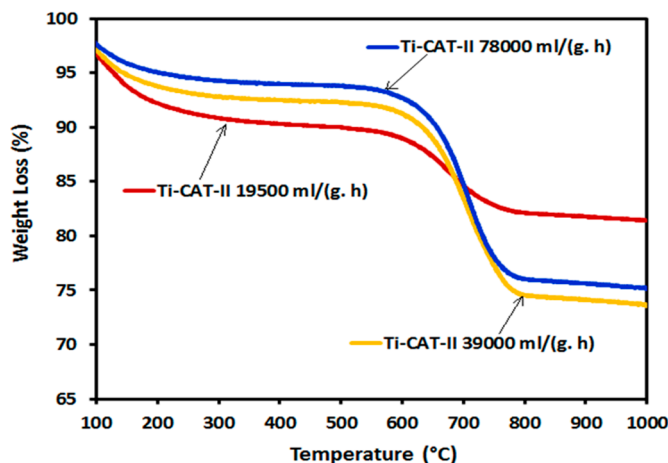


Figure 9. TGA curves for Ti-Cat-II at 19,500, 39,000 and 78,000 mL/(g·h) GHSV values.

From the results of the investigation, it can be inferred that deactivation is expected at all the space velocity investigated, since carbon deposit was evident; however, at 19,500 mL/(g·h) space velocity, the catalyst will stay active for a longer time than at 39,000 and 78,000 mL/(g·h).

2.12. Effect of Different CO₂/CH₄ Ratios

The mole ratio of CO₂ to CH₄ was changed at a fixed total flow rate to study the performance of Ti-CAT-II catalyst when CH₄ was supposed to act as the limiting reagent in excess of CO₂ at 700 °C and 39,000 mL g⁻¹ h⁻¹ GHSV. The results are shown in Figure 10a–c. The highest CH₄ conversion of about 78% was obtained when CO₂ was 20% in excess of CH₄, while the least conversion of CH₄ (~43%) resulted when the amount of CO₂ was 50% of the required stoichiometric amount in the feed. This observation was expected, as CH₄ would have enough CO₂ to undergo dry reforming. On the other hand, the highest CO₂ conversion of (~90%) was observed when CO₂ was the limiting reagent. This observation could be due to excess CH₄ present in the feed. The CO₂ conversion was reduced with the reaction time-on-stream. Such observation could be ascribed to the disproportionation of carbon monoxide into CO₂ and graphite, a transformation known as the Boudouard reaction:



Comparing the different CO₂/CH₄ ratios, it was observed that CH₄ conversion increased with the ratio up to 1.2 (i.e., 0.5 < 1.0 < 1.2) and then declined slightly at 1.5. However, the conversion for CO₂ was observed to decrease as the ratio increased (i.e., 1.5 < 1.2 < 1.0 < 0.5).

Figure 10c displays the H₂/CO mole ratio results. It was observed that at the lowest CO₂/CH₄ mole ratio, the H₂/CO mole ratio was greater than one. This observation could be owing to the insufficient amount of CO₂ for complete dry reforming of the available CH₄ and to the thermal decomposition of unreformed CH₄, giving more H₂ than the stoichiometric amount. Moreover, the Boudouard reaction might contribute to the increase of hydrogen production, because the formed CO₂ from Boudouard reaction would shift the DRM equilibrium to the product side.

On the other hand, H₂/CO mole ratio was close to one of the cases where CO₂ was in excess of CH₄, where it was noticed that the H₂/CO mole ratio increased with the reaction time-on-stream. Once again, the Boudouard reaction might be responsible for such observation.

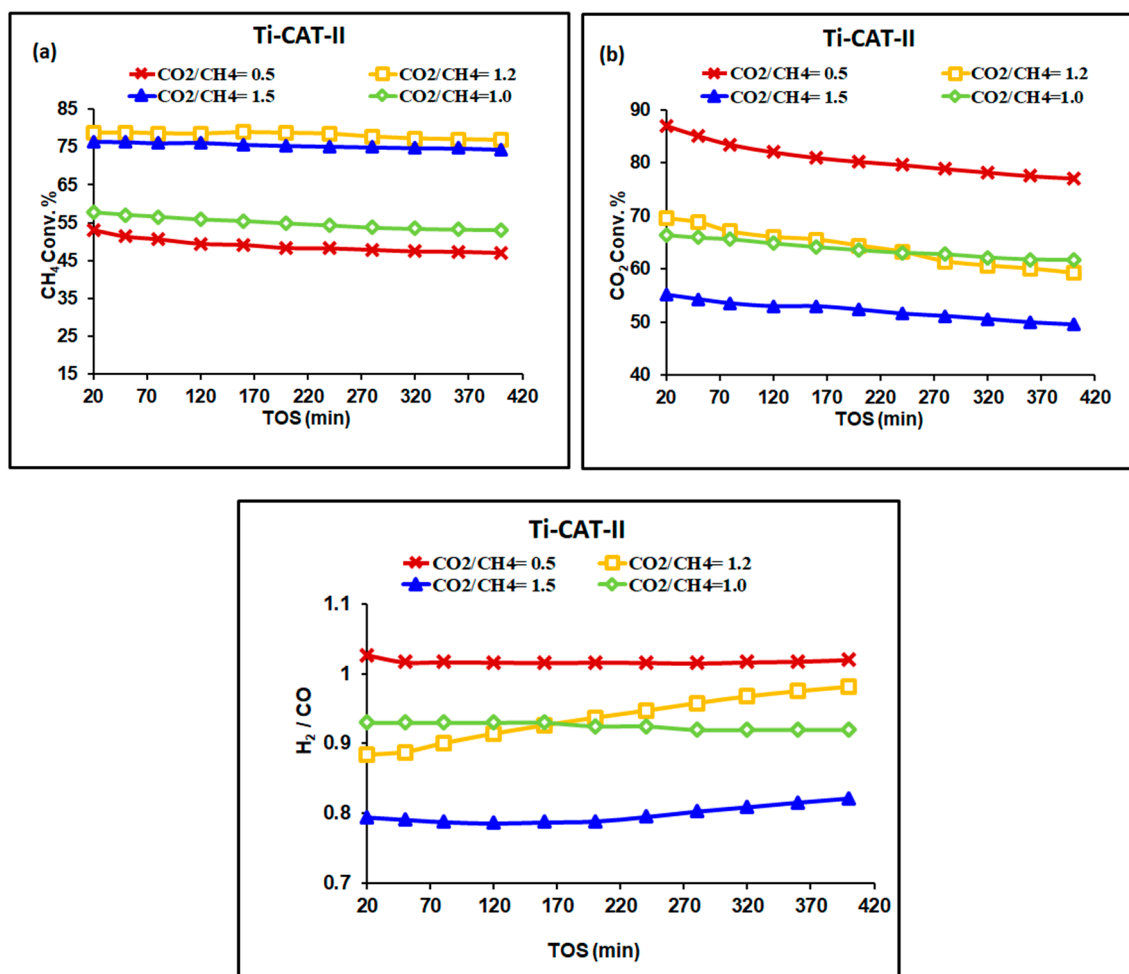


Figure 10. (a) CH₄ (b) CO₂ conversions, and (c) H₂/CO ratio for different CO₂/CH₄ ratio over Ti-CAT-II.

3. Experimental Section

3.1. Materials

Nickel nitrate hexahydrate [Ni(NO₃)₂·6H₂O, 98%, Alfa Aesar], cerium nitrate hexahydrate [Ce(NO₃)₃·6H₂O, 99.0% assay on Ce basis, general purpose reagent, BDH], magnesium acetate tetra-hydrate [Mg(O₂CCH₃)₂·4H₂O, 99.5–102.0%, Merck & Co., Inc., Kenilworth, NJ, USA] were commercially available and were used without further purification. γ -Alumina doped with titania (3.0 wt. % TiO₂/ γ -Al₂O₃) in the shape of pellets, was a gift from Tiancun Xiao, Senior Research Fellow, Inorganic Chemistry Laboratory, Oxford University. Ultrapure deionized water (18.2 M Ω .cm) was obtained from a Milli-Q water purification system (Millipore, Burlington, MA, USA).

3.2. Catalyst Preparation

The required amounts of Ni(NO₃)₂·6H₂O, Ce(NO₃)₃·6H₂O, Mg(O₂CCH₃)₂·4H₂O, and support were mixed and were ground together to fine powder by pestle and mortar. A small amount of ultrapure water was used to convert the solid mixture into a paste, which was spun mechanically until dryness. The paste and spinning process was repeated three times. The final solid was calcined in a digital, programmed muffle furnace at 600 °C for three hours by ramping temperature from room temperature by a rate of 3.0 °C/min. The notation of the prepared catalyst samples and their wt. % loadings of nickel oxide, ceria, and magnesia at 600 °C calcination are given below in Table 4.

Table 4. Prepared catalyst samples and the wt. % of their composition.

Catalyst	Concentration, wt. %		
	NiO	CeO ₂	MgO
Ti-CAT-I	5.0	10.0	1.0
Ti-CAT-II	5.0	10.0	0.0
Ti-CAT-III	5.0	0.0	1.0
Ti-CAT-IV	0.0	10.0	1.0
Ti-CAT-V	5.0	0.0	0.0
Ti-CAT-VI	0.0	10.0	0.0

3.3. Catalyst Characterization

The metallic component composition of all catalysts was determined by an Agilent 7800 inductively coupled plasma mass spectrometry (ICP) at the laboratory of IDAC Merieux NutriSciences, Riyadh, Saudi Arabia. Carbon deposition on the used catalysts was measured by thermogravimetric analysis (TGA) under air by using a Shimadzu TGA-51 (Shimadzu Corp., Kyoto, Japan). A certain amount from the spent catalyst (10 mg) was subjected to heat treatment within the temperature range 25 °C–1000 °C. Ramping temperature was maintained at 20 °C/min. Temperature programmed oxidation (TPO) was performed in an oxidative atmosphere to determine the kind of carbon deposited over the surface of the catalyst using Micromeritics AutoChem II over a temperature range of 50–800 °C under a flow of 10% O₂/He mixture at 40 mL/min. The spent catalyst was first pretreated in the presence of high purity Argon at 150 °C for 30 min and subsequently cooled to room temperature. The Brunauer-Emmet-Teller technique was adopted in calculating the surface area per unit mass of the samples using a device that analyses surface area and porosity, i.e., Micromeritics Tristar II 3020 (Micromeritics Instrument Corporation, Norcross, GA, USA). For nitrogen physisorption measurements, an amount of 0.20–0.30 g weighed from the catalyst was subjected to degassing at 300 °C for three hours prior to analysis. The reducibility of the fresh catalysts was determined by the Micromeritics AutoChem II (Micromeritics Instrument Corporation, Norcross, GA, USA). A sample weight of 75.0 mg was analyzed. Samples were first heated under argon (99.9%) at 150 °C for 30 min, thereafter cooled to 25 °C. Afterwards, samples were heated to 1000 °C at 10 °C/min by allowing the flow of 10% H₂/Ar gas at 40 mL/min. A thermal conductivity detector (TCD) was used to follow the H₂ consumption. Temperature programmed desorption of carbon dioxide (CO₂-TPD) and CO pulse chemisorption measurements were obtained from an automatic chemisorption equipment (Micromeritics AutoChem II 2920) with a TCD. At the start, a 70 mg sample was heated at 200 °C for 1 h under helium (He) flow to remove adsorbed components. Then, CO₂ adsorption was carried out at 50 °C for 60 min in the flow of He/CO₂ gas mixture (90/10 L/L) with a flow rate of 30.0 mL/min. Afterwards, a linear temperature rise at a rate of 10 °C/min until 800 °C was registered by the TCD of CO₂ desorption signal. The nickel metallic surface area and dispersion were determined by H₂ pulse chemisorption by using Micromeritics AutoChem II. A sample of 50.0 mg was heated to 150 °C under vacuum for sixteen hours. The sample was then transferred to the sample tube and was heated at temperature rate of 10.0 °C/min to 400 °C under flow rate of 10.0 mL/min of 10% H₂/Ar for one hour. The sample was then flushed with highly pure Ar for one hour at 400 °C. The temperature was then reduced to 70.0 °C and pulses of H₂ gas were introduced for one hour for determining the H₂ uptake. X-ray powder diffraction patterns for the samples were recorded on a Bruker D8 Advance (Bruker, Billerica, MA, USA) XRD diffractometer by using Cu K_α radiation source and a nickel filter, operated at 40 kV and 40 mA. The step size and scanning range of 2θ for analysis was set to 0.01° and 5–100°, respectively. The present phases were documented using standard powder XRD cards (JCPDS). Catalyst morphology was studied using JEOL JSM-7100F (JEOL, Tokyo, Japan) (field emission scanning electron microscope, equipped with energy-dispersive X-ray spectroscopy (EDXS) for surface elemental analysis.

3.4. Catalytic Performance

Methane reforming reaction was accomplished in a fixed-bed tubular stainless-steel micro-reactor (ID = 9 mm) at atmospheric pressure. The reactor system was provided by Process Integral Development (Process Integral Development Eng & Tech SL, Madrid, Spain). Before performing the DRM reaction, a 0.10 g catalyst was activated by H₂ flow of 40 mL/min at 700 °C for 60 min. N₂ gas was then admitted to the reactor for 20 min to remove adsorbed H₂ while the catalyst was kept at reaction temperature (700 °C). Afterwards, feed gases of CH₄, CO₂, and N₂ were injected at flow rates of 30, 30 and 5 mL/min, respectively. The temperature, pressure and reaction variables were inspected through the reactor panel. A GC (Shimadzu Corp., Kyoto, Japan) unit having a thermal conductivity detector and two columns, Porapak Q and Molecular Sieve 5A, was connected in series/bypass connections in order to have a complete analysis of the reaction products. The following equations were used to calculate the CH₄ and CO₂ conversions respectively.

$$\%CH_4 \text{ conversion} = \frac{CH_4 \text{ in} - CH_4 \text{ out}}{CH_4 \text{ in}} \times 100$$

$$\%CO_2 \text{ conversion} = \frac{CO_2 \text{ in} - CO_2 \text{ out}}{CO_2 \text{ in}} \times 100$$

4. Conclusions

This paper investigated the dry reforming of methane, CH₄, over Ti-CAT-V catalyst, and the effects of promoters such as CeO₂ and MgO, on the catalytic activity and stability of the catalyst. The promoter loading was 10.0 wt. % and 1.0 wt. % for CeO₂ and MgO, respectively. Promoted Ti-CAT-V catalyst showed better conversion of both CH₄ and CO₂ than the un-promoted counterpart. Ti-CAT-II had the highest CH₄ and CO₂ conversion of about 55% and 64% respectively, while no reaction was observed for Ti-CAT-VI and Ti-CAT-IV. It can be inferred from the improved performance of the promoted catalysts that the promoters had a positive influence on the textural properties, metal support interaction and reduction behavior of the catalyst. These impacts of promoters were well shown by the characterization techniques used. From the thermogravimetric analysis, un-promoted catalyst gave the lowest carbon deposition. The promoted catalyst, especially by Ce, with higher amounts than 10% was found to have the highest carbon formation. This result implied that the promoters enhanced the activity performance of the catalyst, resulting in the formation of graphitic carbon, and hence, were not effective in boosting the stability via reduction of carbon deposition relative to the un-promoted catalyst. The TPO investigation indicated the types of carbon formed, which include atomic, amorphous, and graphitic carbon.

Ti-CAT-V was selected for further investigation at different GHSVs and subsequently at various CO₂/CH₄ ratios. An inverse relationship between GHSV and catalytic activity was observed. A GHSV of 19,500 $\frac{\text{feed flow rate}}{\text{mass of cat.}} \left(\frac{\text{mL}}{\text{g} \cdot \text{h}} \right)$ and CO₂/CH₄ ratio of 0.5 gave the best results.

Supplementary Materials: The following are available online at <http://www.mdpi.com/2073-4344/9/2/188/s1>, Figure S1: XRD patterns of fresh catalysts.

Author Contributions: A.S.F., A.H.F, S.O.K., R.A. (Rasheed Alrasheed), R.A. (Rawan Ashamari) and A.B. carried out all experiments and characterization tests as well as shared in the analysis of the data and shared in the writing of the manuscript. A.S.F, S.O.K, A.E.A and A.B. wrote the paper and shared data analysis. A.H.F and A.A.I. contributed in writing the paper and edited it.

Funding: This research was funded by the Deanship of Scientific Research at King Saud University, Project No. RGP-119.

Acknowledgments: The authors would like to express their sincere appreciation to the Deanship of Scientific Research at King Saud University for its funding for this research group project No. (RGP-119).

Conflicts of Interest: The authors declare no conflict of interest.

References

1. Albarazi, A.; Beaunier, P.; Da Costa, P. Hydrogen and syngas production by methane dry reforming on SBA-15 supported nickel catalysts: On the effect of promotion by Ce_{0.75}Zr_{0.25}O₂ mixed oxide. *Int. J. Hydrogen Energy* **2013**, *38*, 127–139. [[CrossRef](#)]
2. Bao, Z.; Lu, Y.; Han, J.; Li, Y.; Yu, F. Highly active and stable Ni based bimodal pore catalysts for dry reforming of methane. *Appl. Catal. A Gen.* **2015**, *491*, 116–126. [[CrossRef](#)]
3. Buelens, L.C.; Galvita, V.V.; Poelman, H.; Detavernier, C.; Marin, G.B. Super-dry reforming of methane intensifies CO₂ utilization via Le Chatelier's principle. *Science* **2016**, *354*, 449–452. [[CrossRef](#)] [[PubMed](#)]
4. Julián-Durán, L.M.; Ortiz-Espinoza, A.P.; El-Halwagi, M.M.; Jiménez-Gutiérrez, A. Techno-economic assessment and environmental impact of shale gas alternatives to methanol. *ACS Sustain. Chem. Eng.* **2014**, *2*, 2338–2344.
5. Schulz, H. Short history and present trends of Fischer-Tropsch synthesis. *Appl. Catal. A Gen.* **1999**, *186*, 3–12. [[CrossRef](#)]
6. Sheu, E.J.; Mokheimer, E.M.A.; Ghoniem, A.F. A review of solar methane reforming systems. *Int. J. Hydrogen Energy* **2015**, *40*, 12929–12955. [[CrossRef](#)]
7. Barelli, L.; Bidini, G.; Gallorini, F.; Servili, S. Hydrogen production through sorption-enhanced steam methane reforming and membrane technology. *Energy* **2008**, *33*, 554–570. [[CrossRef](#)]
8. Hyunjin, J.; Junghun, L.; Eunyeong, C.; Ilsung, S. Hydrogen production from steam reforming using an indirect heating method. *Int. J. Hydrogen Energy* **2018**, *43*, 3655–3663.
9. Cyril, P.; Wenhao, F.; Mickaël, C.; Sébastien, P.; Louise, J.D. Steam reforming, partial oxidation and oxidative steam reforming for hydrogen production from ethanol over cerium nickel based oxyhydride catalyst. *Appl. Catal. A Gen.* **2016**, *518*, 78–86.
10. Youstri, M.A.W.; Mohamed, M.E.G.; Nader, R.A. Steam and partial oxidation reforming options for hydrogen production from fossil fuels for PEM fuel cells. *AEJ* **2012**, *51*, 69–75.
11. Devin, M.W.; Sandra, L.P.; John, T.W.; John, N.K. Synthesis gas production to desired hydrogen to carbon monoxide ratios by tri-reforming of methane using Ni–MgO–(Ce,Zr)O₂ catalysts. *Appl. Catal. A Gen.* **2012**, *445–446*, 61–68.
12. Linus, A.S.; Lea, C.S.K.; Karla, H.D.; Stephan, A.S.; Johannes, A.L. On the coke deposition in dry reforming of methane at elevated pressures. *Appl. Catal. A Gen.* **2015**, *504*, 599–607.
13. Drif, A.; Bion, N.; Brahmi, R.; Ojala, S.; Pirault-Roy, L.; Turpeinen, E.; Seelam, P.K.; Keiski, R.L.; Epron, F. Study of the dry reforming of methane and ethanol using Rh catalysts supported on doped alumina. *Appl. Catal. A Gen.* **2015**, *504*, 576–584. [[CrossRef](#)]
14. Jabbour, K.; El Hassan, N.; Casale, S.; Estephane, J.; El Zakhem, H. Promotional effect of Ru on the activity and stability of Co/SBA-15 catalysts in dry reforming of methane. *Int. J. Hydrogen Energy* **2014**, *39*, 7780–7787. [[CrossRef](#)]
15. Du, X.; France, L.J.; Kuznetsov, V.L.; Xiao, T.; Edwards, P.P.; AlMegren, H.; Bagabas, A. Dry Reforming of Methane Over ZrO₂-Supported Co–Mo Carbide Catalyst. *Appl. Petrochem. Res.* **2014**, *4*, 137–144. [[CrossRef](#)]
16. France, L.J.; Du, X.; Almuqati, N.; Kuznetsov, V.L.; Zhao, Y.; Zheng, J.; Xiao, T.; Bagabas, A.; Almegren, H.; Edwards, P.P. The Effect of Lanthanum Addition on The Catalytic Activity of γ -Alumina Supported Bimetallic Co–Mo Carbides for Dry Methane Reforming. *Appl. Petrochem. Res.* **2014**, *4*, 145–156. [[CrossRef](#)]
17. Tao, X.; Wang, G.; Huang, L.; Li, X.; Ye, Q. Effect of Cu–Mo Activities on the NiCuMo/Al₂O₃ Catalyst for CO₂ Reforming of methane. *Catal. Lett.* **2016**, *146*, 2129–2138. [[CrossRef](#)]
18. Budiman, A.W.; Song, S.-H.; Chang, T.-S.; Shin, C.-H.; Choi, M.-J. Dry reforming of methane over cobalt catalysts: A literature review of catalyst development. *Catal. Surv. Asia* **2012**, *16*, 183–197. [[CrossRef](#)]
19. Park, J.H.; Lee, D.; Lee, H.C.; Park, E.D. Steam reforming of liquid petroleum gas over Mn-promoted Ni/ γ -Al₂O₃ catalysts. *Korean J. Chem. Eng.* **2010**, *27*, 1132–1138. [[CrossRef](#)]
20. Gao, X.; Bare, S.R.; Fierro, J.L.G.; Banares, M.A.; Wachs, I.E. Preparation and in-Situ Spectroscopic Characterization of Molecularly Dispersed Titanium Oxide on Silica. *J. Phys. Chem. B* **1998**, *102*, 5653–5666. [[CrossRef](#)]
21. Klein, S.; Thorimbert, S.; Maier, W.F. Amorphous microporous titania–silica mixed oxides: Preparation, characterization, and catalytic redox properties. *J. Catal.* **1996**, *163*, 476–488. [[CrossRef](#)]

22. Miller, J.B.; Ko, E.I. Control of mixed oxide textural and acidic properties by the sol-gel method. *Catal. Today* **1997**, *35*, 269–292. [[CrossRef](#)]
23. Niu, F.; Li, S.; Zong, Y.; Yao, Q. Catalytic Behavior of Flame-Made Pd/TiO₂ Nanoparticles in Methane Oxidation at Low Temperatures. *J. Phys. Chem. C* **2014**, *118*, 19165–19171. [[CrossRef](#)]
24. Tauster, S.J.; Fung, S.C.; Baker, R.T.K.; Horsely, J.A. Partial Oxidation of Methane to Synthesis Gas over Ru/TiO₂ Catalysts: Effects of Modification of the Support on Oxidation State and Catalytic Performance. *Science* **1981**, *211*, 1121–1125. [[CrossRef](#)]
25. Shamskar, F.R.; Meshkani, F.; Rezaei, M. Preparation and characterization of ultrasound-assisted co-precipitated nanocrystalline La-, Ce-, Zr-promoted Ni-Al₂O₃ catalysts for dry reforming reaction. *J. CO₂ Util.* **2017**, *22*, 124–134. [[CrossRef](#)]
26. Jang, W.J.; Jung, Y.S.; Shim, J.O.; Roh, H.S.; Yoon, W.L. Preparation of a Ni-MgO-Al₂O₃ catalyst with high activity and resistance to potassium poisoning during direct internal reforming of methane in molten carbonate fuel cells. *J. Power Sources* **2018**, *378*, 597–602. [[CrossRef](#)]
27. Ahmed, S.A.A.; Anis, H.F.; Ahmed, E.A. Effects of Selected Promoters on Ni/Y-Al₂O₃ Catalyst Performance in Methane Dry Reforming. *Chin. J. Catal.* **2011**, *32*, 1604–1609.
28. Zhu, F.; Zhang, H.; Yan, X.; Yan, J.; Ni, M.; Li, X.; Tu, X. Plasma-catalytic reforming of CO₂-rich biogas over Ni/γ-Al₂O₃ catalysts in a rotating gliding arc reactor. *Fuel* **2017**, *199*, 430–437. [[CrossRef](#)]
29. Mei, D.; Ashford, B.; He, Y.-L.; Tu, X. Plasma-catalytic reforming of biogas over supported Ni catalysts in a dielectric barrier discharge reactor: Effect of catalyst supports. *Plasma Process. Polym.* **2017**, *14*, 1600076. [[CrossRef](#)]
30. Akbari, E.; Alavi, S.M.; Rezaei, M. Synthesis gas production over highly active and stable nanostructured NiMgOAl₂O₃ catalysts in dry reforming of methane: Effects of Ni contents. *Fuel* **2017**, *194*, 171–179. [[CrossRef](#)]
31. Sudarsanam, P.; Hillary, B.; Deepa, D.K.; Amin, M.H.; Mallesham, B.; Reddy, B.M.; Bhargava, S.K. Highly efficient cerium dioxide nanocube-based catalysts for low temperature diesel soot oxidation: The cooperative effect of cerium- and cobalt-oxides. *Catal. Sci. Technol.* **2015**, *5*, 3496–3500. [[CrossRef](#)]
32. Li, R.; Qian, R.; Jiang, Z.-T. Synthesis of high specific surface area titania monolith by addition of poly (ethylene oxide). *Mater. Res. Innov.* **2015**, *19*, S8–S136. [[CrossRef](#)]
33. Liu, Y.; Lan, K.; Bagabas, A.A.; Zhang, P.; Gao, W.; Wang, J.; Sun, Z.; Fan, J.; Elzatahry, A.A.; Zhao, D. Ordered Macro/Mesoporous TiO₂ Hollow Microspheres with Highly Crystalline Thin Shells for High-Efficiency Photoconversion. *Small* **2016**, *12*, 860–867. [[CrossRef](#)] [[PubMed](#)]
34. Pudukudy, M.; Yaakob, Z.; Akmal, Z.S. Direct decomposition of methane over SBA-15 supported Ni, Co and Fe based bimetallic catalysts. *Appl. Surf. Sci.* **2015**, *330*, 418–430. [[CrossRef](#)]
35. Siew, K.W.; Lee, H.C.; Gimbin, J.; Chin, S.Y.; Khan, M.R.; Taufiq-Yap, Y.H.; Cheng, C.K. Syngas production from glycerol-dry (CO₂) reforming over La-promoted Ni/Al₂O₃ catalyst. *Renew. Energy* **2015**, *74*, 441–447. [[CrossRef](#)]
36. Wang, W.; Wang, S.P.; Ma, X.B.; Gong, J.L. Recent advances in catalytic hydrogenation of carbon dioxide. *Chem. Soc. Rev.* **2011**, *40*, 3703–3727. [[CrossRef](#)] [[PubMed](#)]
37. Wu, J.; Fang, Y.; Wang, Y.; Zhang, D.K. Combined coal gasification and methane reforming for production of syngas in a fluidized-bed reactor. *Energy Fuel* **2005**, *19*, 512–516. [[CrossRef](#)]
38. Hao, Z.; Zhu, Q.; Jiang, Z.; Hou, B.; Li, H. Characterization of aerogel Ni/Al₂O₃ catalysts and investigation on their stability for CH₄-CO₂ reforming in a fluidized bed. *Fuel Process. Technol.* **2009**, *90*, 113–121. [[CrossRef](#)]
39. Lalit, S.G.; Guido, S.J.S.; Valero-Romero, M.J.; Mallada, R.; Santamaria, J.; Stankiewicz, A.I.; Stefanidis, G.D. Synthesis, characterization, and application of ruthenium-doped SrTiO₃ perovskite catalysts for microwave-assisted methane dry reforming. *Chem. Eng. Process. Process Intensif.* **2018**, *127*, 178–190.

